Histol Histopathol (2017) 32: 1281-1291

http://www.hh.um.es

Histology and Histopathology

From Cell Biology to Tissue Engineering

Expression profiles of angiogenesis in two high grade chondrosarcomas: A xenotransplant experience in nude mice

Francisco Giner[1], José Antonio López-Guerrero[2], Isidro Machado[1,3], Zaida García-Casado[2], Antonio Fernández-Serra[2], Amando Peydró-Olaya[1] and Antonio Llombart-Bosch[1]

[1]Department of Pathology, Universitat de València Estudi General (UVEG), [2]Laboratory of Molecular Biology and [3]Department of Pathology, Fundación Instituto Valenciano de Oncología (FIVO), Valencia, Spain

Summary. Background. Chondrosarcomas (Chs) are malignant cartilage-forming tumors that represent the third most common malignant solid tumor of bone in adults. Angiogenesis is a major factor for tumor growth and metastasis. Our aim was to make a histological, immunohistochemical, ultrastructural and molecular characterization of the neovascularization established between xenotransplanted Chs and the host during the initial phases of growth in nude transfer, in order to find potential markers for distinguishing between high grades II and III Chs. Methods. two xenotransplanted high grade human Chs were evaluated. Tumor pieces were implanted subcutaneously on the backs of 14 athymic Balb-c nude mice. The animals were sacrificed 24, 48, and 96 hours; and 7, 14, 21 and 28 days after implantation. Two grade I Chs were also transferred in nude but did not grow. Results. Morphological differences were apparent between these two Chs during the early stages of neoplastic growth. Immunohistochemistry demonstrated overexpression of pro-angiogenic factors 24h-48h after tumor implantation. Additionally, neoplastic cells co-expressed chemokines (CXCL9, CXCL10 and GRO) and their receptors. Molecular studies showed two expression profiles, revealing an early and a late phase in the angiogenic process. Conclusion. High grade Chs demonstrated two different stages of induced angiogenesis, with an intimate association between structural and molecular events that might explain the different aggressive biological behavior of grade II and III Chs. The present model may be useful for testing the effect of anti-angiogenic drugs.

Key words: Chondrosarcoma, Angiogenesis, Nude mice xenograft, Chemokines

Offprint requests to: Antonio Llombart-Bosch, Department of Pathology, University of Valencia, Avda. Blasco Ibáñez, 15, 46010 Valencia, Spain. e-mail: antonio.llombart@uv.es

DOI: 10.14670/HH-11-880

Introduction

Chondrosarcomas (Chs) are malignant cartilage-forming tumors that represent the third most common malignant solid tumor of bone. With an incidence of 1:50,000, Chs typically occur in adults in their 5th to 7th decade of life (Hogendoorn et al., 2013). As Chs do not respond well to chemo- or radiotherapy, there is an urgent need for modelling systems in pre-clinical research to evaluate new targeted treatment strategies for Ch (Bovee et al., 2010). Conventional Ch can be classified in two groups according to the location in bone: central Ch, located inside the medullar cavity; and peripheral Ch, located on the surface of the bone (Rozeman et al., 2006). The histopathology is quite similar in both locations and is classified as: Grade I, II or III. In Grade II Ch the nuclei are of moderate size with increased cellularity and low mitotic rate. Grade III Ch reveals large nuclei in areas with increased cellularity and anaplasia with moderate mitotic rate and scant chondroid differentiation, and a more rich myxoid matrix(Rozeman et al., 2006; Hogendoorn et al., 2013). For a number of authors, Ch Grades II and III can be grouped as high grade Ch with no major clinical differences (Bovee et al., 2010; van Oosterwijk et al., 2013).

In recent years, much research has focused on the role of angiogenesis in tumor development, growth,

invasion and metastasis (Carmeliet and Jain, 2011; Hanahan and Weinberg, 2011). It is clear that tumor angiogenesis is the result of an imbalance between pro-angiogenic and anti-angiogenic factors. The threshold of change in favor of pro-angiogenesis is considered the angiogenic switch. Several angiogenic factors and chemokines are related with angiogenic mechanisms and have been studied in different tumor types (Berghuis et al., 2011; Carmeliet and Jain, 2011; Pinto et al., 2014). We recently communicated these findings in an osteosarcoma nude mice model (Giner et al., 2015). The angiogenic process presents two different phases of tumor growth. An initial induction phase, in which new unstable vessels are built, followed by a remodeling phase, in which blood vessels are stabilized (Llombart-Bosch et al., 2003). At this point, hypoxia activates the angiogenic process through the well-known hypoxia inducible transcription factors (HIF) that induce the expression of several tumor-derived cytokines, such as vascular endothelial growth factors (VEGF) or fibroblast growth factors (FGF) (Carmeliet and Jain, 2011) and some chemokines (CXCL9, CXCL10 and GRO) with their respective receptors (CXCR3 and CXCR2) (Link et al., 1986; DuBois and Demetri, 2007; Berghuis et al., 2011). Consequently, considerable interest has been generated in the therapeutic potential of targeting the growth of new vessels (anti-angiogenesis) and the capacity to control those that have been formed (vascular targeting) (Link et al., 1986; Mantadakis et al., 2001). Hence, identifying the main elements involved in the initiation of angiogenesis in Chs is fundamental to understanding this process in this particular tumor and to derive information regarding potential candidates for effective targeted therapy.

Animal models have been widely used in the study of tumor angiogenesis (Llombart-Bosch et al., 2003; DuBois and Demetri, 2007; Machado et al., 2008). We employed a nude mice model to study the early stages of this process in two xenotransplanted high grade human Chs. Two grade I Chs did not grow in our mice xenograft model (Machado et al., 2008) and could not be used in this experiment. A fact which puts into question the true malignant nature of this neoplasm.

Our aim was to characterize through histological, immunohistochemical, ultrastructural and molecular studies the neovascularization established between the xenotransplanted Chs and the host at initial stages of neoplastic growth, and to determine the possible variables in the immunohistochemical and molecular expression patterns that might provide some biological markers for distinguishing between high grades II and III Chs, leading to a more effective and specific targeted therapy.

Material and methods

Samples

Two xenotransplanted high grade human Chs were evaluated: Nu465 and Nu467. Nu465, a Grade II Chs, came from a 25-year-old male referred to our hospital complaining of pain in the left lumbar area. The tumor was resected and collected for histopathologic and ultrastructural characterization with genetic studies. The original tumor was implanted subcutaneously on the back of male nude mice (Nu465) and maintained for several generations as previously published (Calabuig-Farinas et al., 2012). Nu467, a Grade III Chs came from a well-established and characterized solid tumor and Ch cell line (ch-2879), the morphological and clinical characteristics of which have also been communicated (Gil-Benso et al., 2003). The tumor was also implanted subcutaneously on the back of male nude mice (Nu467) and maintained for several generations as described above. In both Chs we divided the passages into three time periods, early passages (from 1st to 5th passage), middle passages (from 6th to 10th passage) and late passages (from 11th to 15th passage). We calculate the average speed of tumor growth in both nude mice passages (Nu465 and Nu467) according to the formula (15 mm/days to next passage), the mice were sacrificed when the tumor reached 15 mm.

Tumor pieces 3-4 mm in size from the first passage of Nu465 and the second passage of Nu467 were implanted subcutaneously on the backs of two sets of athymic Balb-c male nude mice (n=14 each). The animals were sacrificed 24, 48, and 96 hours; and 7, 14, 21 and 28 days after implantation. Tissue samples were fixed in 10% formaldehyde, paraffin embedded, and stained with hematoxylin and eosin (H&E) for histological analysis. Additional samples were fixed with glutaraldehyde (2%) for electron microscopy and non-fixed samples were collected for molecular analysis. Approval for animal experimentation was obtained from the Ethics Committee of the Universitat de València Estudi General (UVEG).

Immunohistochemistry

Immunohistochemistry was carried out using an indirect peroxidase method on paraffin sections. Antigen retrieval was performed with heat-induced epitope retrieval (autoclave at 1.5 atmospheres for 3 minutes in citrate buffer). Bound antibodies were visualized by an avidin-biotin-peroxidase procedure (LSAB DAKO®). Negative controls consisted of substitution of the primary antibody with a saline phosphate buffer. Table 1 lists the antibodies, their source of origin, and dilutions. Immunoreactivity was defined as follows: negative, fewer than 5% of tumor cells stained; weakly positive (1+), between 5 and 10% of tumor cells stained; moderately positive (2+), between 10% and 50% of tumor cells stained; and strongly positive (3+), more than 50% of tumor cells stained. Ki67 expression was considered: weakly positive (1+), between 1 and 10% of tumor cells stained; moderately positive (2+), between 10% and 20% of tumor cells stained; and strongly

positive (3+), more than 20% of tumor cells stained. All sections were independently evaluated by three pathologists (FG, IM and ALLB) and in cases of disagreement, the score was determined by consensus. Double-immunofluorescence staining was carried out by an indirect method on paraffin sections. Antigen retrieval was performed with heat-induced epitope retrieval as described above. We used primary (Dako® and R&DSystems®) and secondary antibodies (Alexa-Fluor®) in accordance with the manufacturer's instructions. Stained sections were examined with a confocal microscope (Olympus FV1000®). Immunoreactivity was scored following conventional immunohistochemistry criteria. We assessed positivity in nucleus, cytoplasm and/or membrane according to each antibody (Table 1). All sections were evaluated independently by three pathologists (FG, IM and ALLB), and in cases of disagreement, the score was determined by consensus.

Electron microscopy

Tissues for electron microscopy were fixed in glutaraldehyde for 2 hours, washed three times, and stored overnight in 0.1 M cacodylate buffer (pH 7.4). Tissue was post-fixed in 2% sodium-cacodylate buffered osmium tetroxide solution for 1.5 hours and embedded in Eponate 12 (Ted Pella, Redding, Louisiana). After dehydration with increasing concentrations of ethanol, fixed tumor tissues were embedded in propylene oxide Eponate and cut into 1 µm-thick sections. Sections were stained with toluidine blue to select representative fields of the tumor and cultures by light microscopy. Ultrathin sections were made with a Reichert Ultracut Ultramicrotome (Leica, Inc., Deinfield, Illinois), stained with lead citrate and uranyl acetate, and observed under an electron microscope (JEOL JEM 1010, Tokyo).

Molecular biology

RNA was extracted from 50 to 200 mg of tumor tissue obtained from the Nu465 and Nu467 series using the Recover All Total Nucleic Acid Isolation® kit (Ambion, Austin, USA) following the manufacturer's instructions. RNA concentration was measured at 260 and 280 nm using the Nanodrop® 1000 spectrophotometer (Thermo Scientific). RNA integrity was tested by checking the 28S and 18S ribosomal bands on 1 µg of the obtained RNA by gel electrophoresis (1% agarose), staining the gel with ethidium-bromide and visualizing with ultraviolet light.

Reverse transcription was performed using 200 ng of total RNA with the High Capacity cDNA Reverse Transcription Kit® (Applied Biosystems, Foster City, USA). Briefly, cDNA synthesis was carried out in a 20 μl final volume reaction containing 2 μl of RT buffer (10X), 2 μl of random hexamers (10X), 0.8 μl of dNTP Mix (25X), 1 μl of RNAse inhibitor (50U/µl) and 1 μl of MultiScribe™ reverse transcriptase (50U/µl). The thermo cycler program consisted of: 10 min at 25°C, 120 min at 37°C and a final step of 5 min at 85°C. The expression of 96 angiogenesis-related genes was then evaluated by quantitative RT-PCR (qRT-PCR) using micro-fluidic card technology on an ABI 9700HT thermocycler (Applied-Biosystems). These genes included: 5 promoters of angiogenesis, 41 growth factors and their receptors, 15 chemokines and cytokines, 5 adhesion molecules, 17 matrix proteins, matrix proteases and their inhibitors, 6 transcription factors and other 7 genes (Table 1. Supplementary). The expression of each gene was normalized with the *β2-microglobulin* and *18S* genes (Hs99999907_m1 and Hs99999901_s1 assays respectively, Applied Biosystems, Foster City, CA) and relative expression was determined using the mean value of the control samples (tumor before transplantation) as

Table 1. Antibodies used in the experiences.

Marker	Clonality (Clon)	Location	Dilution	Manufacturer	Treatment
Ki-67	Monoclonal (MIB-1)	nuclear	1/50	Dako	Autoclave Citrate Buffer pH6
HIF1 α	Monoclonal (HI α 67)	cytoplasm	1/500	Chemicon	Autoclave EDTA pH8
VEGF	Monoclonal (VG 1)	cytoplasm	1/100	Neomarkers	Autoclave EDTA pH8
VEGFR1	Polyclonal (rabbit)	cytoplasm/membrane	1/400	Santa Cruz	Autoclave Citrate Buffer pH6
VEGRF2	Polyclonal (rabbit)	cytoplasm/membrane	1/400	Santa Cruz	Autoclave Citrate Buffer pH6
VEGFR3	Polyclonal (rabbit)	cytoplasm/membrane	1/400	Santa Cruz	Autoclave Citrate Buffer pH6
PDGFR α	Polyclonal (rabbit)	cytoplasm	1/100	Santa Cruz	Autoclave Citrate Buffer pH6
FGF 2	Polyclonal (rabbit)	cytoplasm	1/200	Santa Cruz	Water bath, high pH Dako
PDGFRβ	Polyclonal (rabbit)	cytoplasm	1/100	Santa Cruz	Autoclave Citrate Buffer pH6
VE- CAD	Polyclonal (goat)	cytoplasm/membrane	1/50	Santa Cruz	Autoclave Citrate Buffer pH6
CXCL9	Polyclonal (goat)	cytoplasm	1/100	R&DSystems	Autoclave Citrate Buffer pH6
CXCL10	Polyclonal (goat)	nuclear/cytoplasm	1/100	R&DSystems	Autoclave Citrate Buffer pH6
GRO	Monoclonal (31716)	cytoplasm	1/200	R&DSystems	Autoclave Citrate Buffer pH6
CXCR3	Monoclonal (2Ar1)	cytoplasm/membrane	1/200	Abcam	Autoclave Citrate Buffer pH6
CXCR2	Polyclonal(mouse)	cytoplasm/membrane	1/20	BioLegend	Autoclave Citrate Buffer pH6
Vimentine	Monoclonal (V9)	cytoplasm	1/300	Novocastra	Autoclave EDTA pH6

calibrator and following the $2^{-\Delta\Delta Ct}$ method (Livak and Schmittgen, 2001).

Cluster analysis was performed using the Gene Expression Pattern Analysis Suite v3.1 (http://gepas3.bioinfo.cipf.es/).

ELISA experiments

Blood samples were also collected for the nude mice series, and serum was evaluated for human and mouse VEGF levels using the RayBio® VEGF ELISA (Enzyme-Linked Immunosorbent Assay) kits (ELH-VEGF-001 and ELM-VEGF-001 for human and mouse respectively) and following the manufacturer's instructions. A microplate luminometer (MultiRead 400®, Anthos, Inc.) was used to determine the VEGF expression levels in pg/ml.

Results

Histological, immunohistochemical and ultrastructural characterization

Nu467 presented a higher average speed of tumor growth in nude mice passages (0.283 mm/day) than Nu465 (0.223 mm/day). In both tumors the average speed of growth in xenografts increased with each passage (Fig. 1).

Both primitive human tumors demonstrated high-grade features such as abundant mitotic figures or an undifferentiated component (Fig. 2).

In the first hours after xenografting, peritumoral hemorrhagic areas with inflammatory infiltration compounded by lymphocytes and neutrophils were observed in both Chs. Small capillaries surrounded the xenograft associated with mesenchymal angioblastic-like cells included in a loose matrix.

Multifocal hypoxic necrosis appeared within the first 24 to 48 h after implantation of Nu467 (Fig. 3D,E). In contrast, a patchy and less extensive necrosis appeared later (48 to 96 h) in Nu465 (Fig. 3A,B). Areas of massive necrosis in both tumors were associated with a lower proliferative index (Fig. 4). Four weeks after xenografting the proliferative index had recovered and necrosis was practically absent (Fig. 3C,F). During the third week after xenografting the inflammatory component decreased and a pseudocapsule appeared in both tumors. At this time newly formed capillary vessels were remodeled and penetrated or sprouted into the tumor (Fig. 3C).

Angiogenic factors represented by the family VEGF and their receptors presented different expression profile in the two Chs. In Nu467, maximum VEGF positivity presented 24h after implantation and was also expressed in the extracellular matrix, while VEGF positivity was lower in Nu465 and appeared 96h after xenografting. VEGFR2 presented a similar expression profile as its ligand, and VEGFR3 was the most positive receptor in both tumors.

Ki67 expression was higher in Nu467 than in Nu465. In both tumors Ki67 was lower in the early stages after tumor xenografting. After the first week, the increase in Ki67 expression was also inversely correlated with HIF1α in both Chs (Fig. 4).

Double-immunofluorescence staining showed chemokine expression (CXCL9, CXCL10 and GRO) in the tumor cell cytoplasm as well as in the extracellular matrix. This was also the case for their receptors (CXCR3 and CXCR2) (Fig. 3G,H,I). Chemokine ligand expression was higher during the first 48 h in both Chs. It is worth mentioning that the chemokine receptors were expressed more constantly at all times compared to their ligands.

Ultrastructurally, we identified two phases in both tumors, but with no notable differences between them. Within the first 96 hours of the experiment no new vessels appeared, and the tumor cells formed lacunar-like spaces filled with isolated erythrocytes, reproducing a "tumor cell vascular-like mimicry" but with no real host endothelial cells (Fig. 5). Isolated tumor permeation from the host angioblasts originating in the capsule occurred within the 2nd and 3rd week of the experiment. These mesenchymal angioblasts appeared isolated or in small groups, loosely dispersed within the tumor matrix, and making close contact with the cytoplasm of the tumor cells. Irregularities appeared in the endothelial configuration of the capillaries, with the presence of poorly developed structures. Basal laminae were absent with intimate continuity of endothelial and tumor cells (Fig. 6A-C). Vascular mosaicism, where chondrosarcomatous cells are in direct contact with the host endothelium configuring a pseudo-capillary filled with erythrocytes, was not observed.

ELISA experiments

Both human and mouse VEGF serum levels were

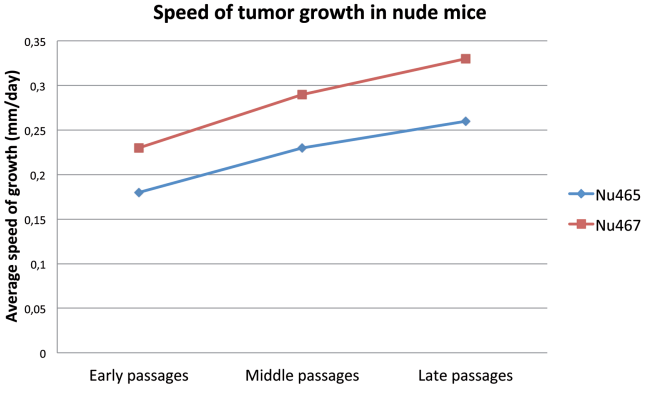

Fig. 1. Speed of tumor growth throughout the xenograft passages in both Chs.

measured by ELISA in the Nu465 and Nu467 series. Human VEGF was not detected. However, mouse serum VEGF levels were higher after the first week in Nu467 and no expression peak was seen in Nu465 (Fig. 7).

qRT-PCR low density arrays of angiogenesis related genes

Gene expression profiles (Fig. 8) in Nu465 at 24 h and 28 days were similar, but differed from those observed at 48 h, and 14 and 21 days. In Nu467 the early phase appeared 24 h after xenografting, and was characterized by the overexpression of genes clearly involved in the induction of angiogenesis, including VEGF, PDGFA, PDGFB, VEGFC and their receptors. In Nu465 the induction phase occurred 48 h after xenografting. Finally, in Nu467 the late phase of the angiogenic process (remodelling phase) appeared during the 1st and 2nd week after xenografting, while in Nu465 this phase appeared later in the 4th week.

RNA samples corresponding to 96h and one week of the Nu465, and to 96h of the Nu467 were not viable for analysis.

Discussion

Angiogenesis is critical for the growth and metastasis of tumors. Early in tumorigenesis, hypoxia activates an angiogenic switch promoting the expression of pro-angiogenic growth factors, such as the VEGF

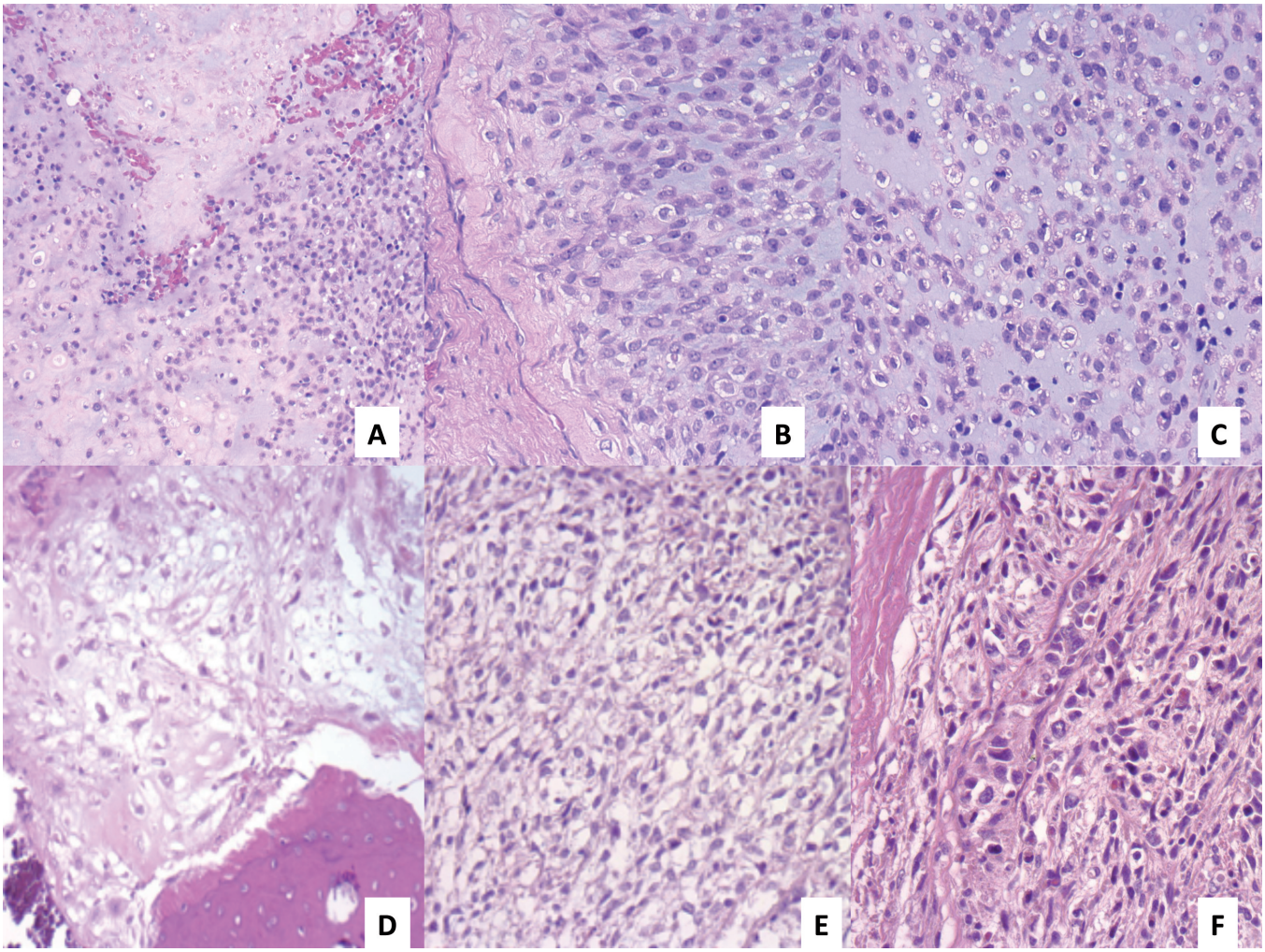

Fig. 2. A-C. Original human Ch of Nu465 (H&E). **D-F.** Original human Ch of Nu467 (H&E). **A.** Presence of abundant tumorigenic capillaries next to tumor cells with necrotic areas. **B.** Chondroblastic tumor cells surrounded by an immature chondroblastic matrix in tumor borderline area with surrounded stroma. **C.** Abundant mitotic figures in a more cellular area. **D.** Presence of chondroblastic cells surrounded by chondroid matrix breaking bone osteoid matrix. **E.** Abundant myxoid degeneration with marked nuclear pleomorphism. **F.** View with undifferentiated areas. A, D, x 20; B, C, E, F, x 40

family, its receptors and HIF1α among others (Hanahan and Weinberg, 2011). Chs have few blood vessels, and consequently represent a difficult target for anti-angiogenic therapies (Kubo et al., 2013). Moreover, unresectable and metastatic Chs are notable for the lack of response to conventional chemo- and radiotherapy, and high grade Ch has a propensity for lung metastasis and poor survival. We constructed an *in vivo* model of two high grade human Chs in nude mice to better understand the early stages of tumor angiogenesis as well as their possible behavior in relation to molecular expression profiles. Improved knowledge of the biology of Chs could support the design of new therapeutic strategies, including anti-angiogenic drugs. HIF1α is a principal regulator of cellular and systemic homeostatic response to hypoxia as it activates many genes, including those involved in angiogenesis (Carmeliet and Jain, 2011). In our model, HIF1α was overexpressed in the early stages, decreasing progressively after one week, indicating that the angiogenic process is constitutively active in the xenotransplanted tumor. HIF1α plays an important role in the angiogenic induction and remodeling phases and has been correlated with microvessel density and poor prognosis in cartilaginous tumors (Boeuf et al., 2010; Chen et al., 2011). Moreover, HIF1α expression is suggested to

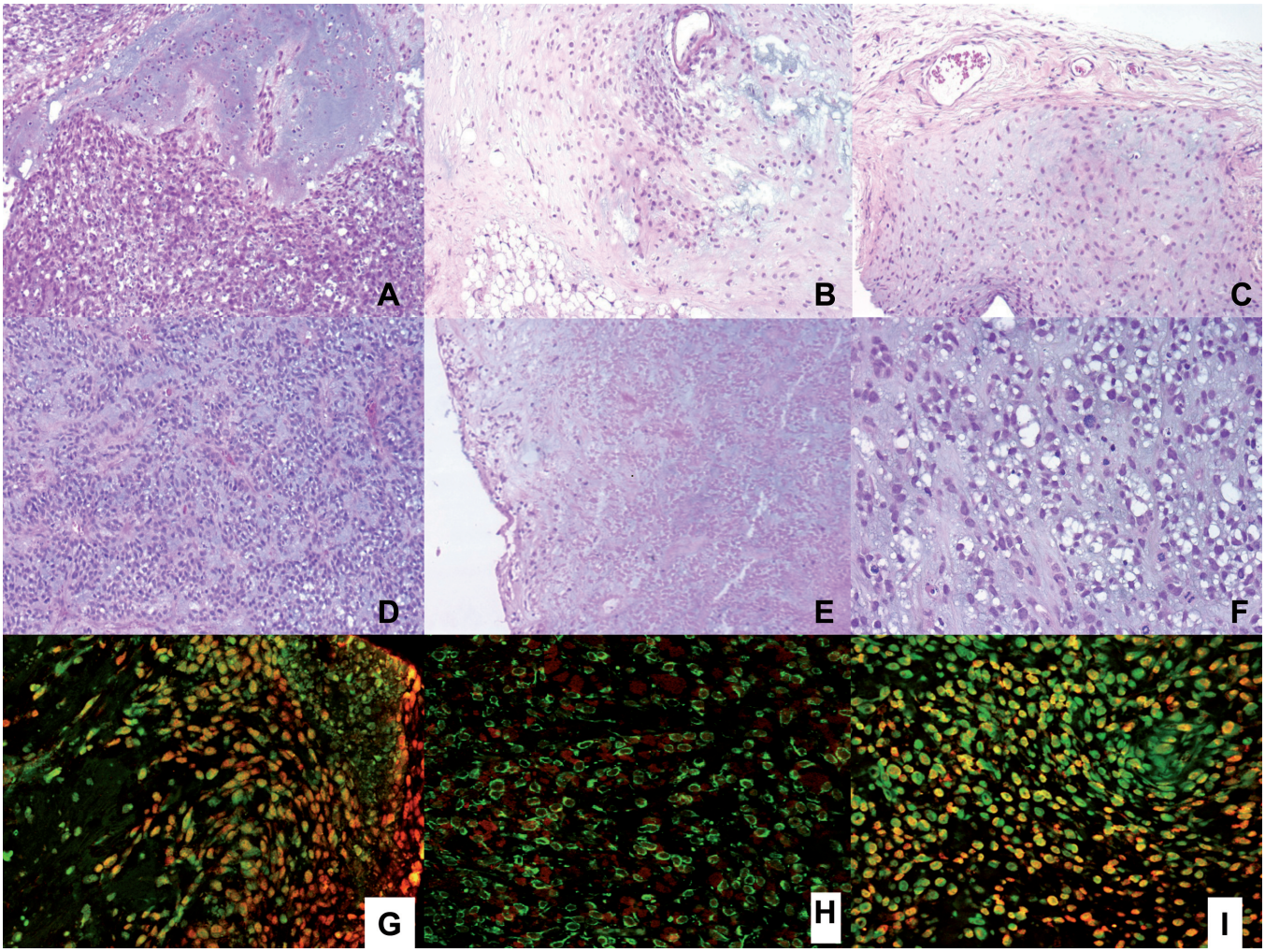

Fig. 3. Nu465: **A.** Focal geographic necrosis 48h after xenografting (H&E). **B.** The necrosis becomes massive 96h after xenografting (H&E). **C.** 28 days after xenografting showing peritumoral pseudocapsule and several remodelled blood vessels (H&E). **D.** Nu467, 48h after xenografting the necrosis is multifocal involving all the tumor (H&E). **E.** The tumor suffers massive necrosis 96h later due to hypoxia and only a thin rim of cells survive at the periphery of the xenograft (H&E). **F.** 28 days after the tumor implantation the Ch-cells recover and present mitosis (H&E). **G.** double-immunofluorescence staining shows intense coexpression with chemokine ligand CXCL9 (red) and its receptor CXCR3 (green) by tumor cells in Nu465 the first 48h after xenografting. **H.** Double-immunofluorescence staining shows intense intra- and extracellular coexpression of GRO (red) in tumor cells marked with vimentin (green) the first week after xenografting in Nu467. **I.** Double-immunofluorescence staining shows coexpression with chemokine ligand GRO (red) and its receptor CXCR2 (green) by tumor cells in Nu465 the first week after xenografting. A-E, x 20; F-I, x 40

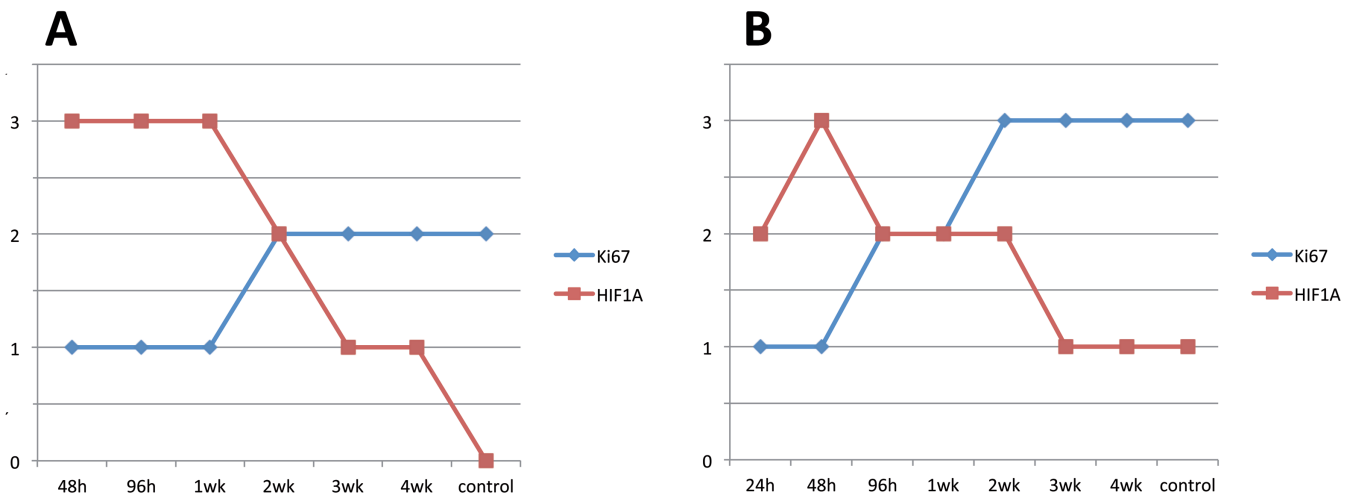

Fig. 4. Immunohistochemical expression of Ki67 with HIF1α over time after xenografting in Nu465 **(A)** and Nu467 **(B)** based upon extent and intensity of cell staining (see text). Sample from 24h in Nu465 was not available for analysis.

result in increased VEGF expression in Ch (Lin et al., 2004). We did not detect human VEGF in the blood of the mice, and the two Chs exhibited different murine VEGF profiles. In Nu465, murine VEGF was expressed steadily without peaks (around 80 pg/ml). However, in Nu467, an increase of murine VEGF was appreciated at 96h (95 pg/ml approx.) and 1 week (around 110 pg/ml) after xenografting. Curiously, VEGF appeared in mice blood some hours later than in chondroblast cells by qRT-PCR studies. These observations suggest that firstly, human VEGF is only locally produced by tumor cells in order to stimulate endothelial cells of the capillaries surrounding the tumor (which was produced in the early phase, during angiogenesis induction); and secondly, that expression of murine VEGF is increased mainly during the late phase, probably associated with the mobilization of angioblastic pluripotent cells from the bone marrow of the mice which will contribute to the angiogenic remodelling within the tumor (Ohba et al., 2014). This finding was confirmed with our electron microscope studies in which two phases of angiogenesis were present, the first induced by the tumor cells producing vascular mimicry, and a second, occurring within the last two weeks of the experiment, due to the proliferation of host angioblastic sprouts which grow into the tumor parenchyme originating early capillaries in close association to tumor cells.

Cluster analysis of our qRT-PCR expression studies also revealed two groups of genes that are clearly separated into two stages corresponding to early angiogenic induction and the later remodelling phases. Possibly, when Ch is more aggressive, both phases appear earlier with higher expression of pro-angiogenic factors, similar to high-grade osteosarcomas (Giner et al., 2015), as occurs in Nu467, a grade III Ch which had a higher average speed of growth in nude mice passages

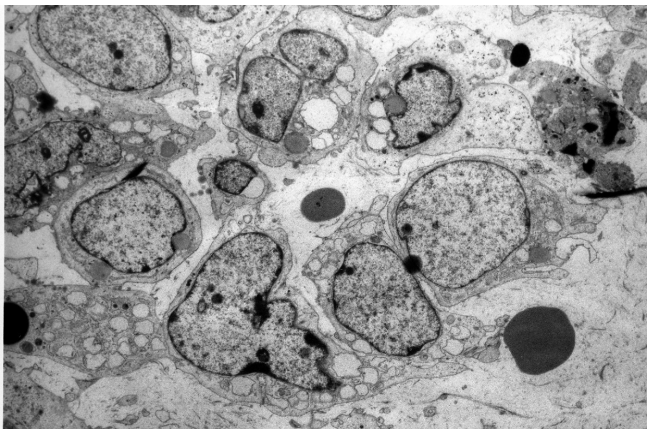

Fig. 5. Electron microscopy of a vascular mimicry in Nu467, 48 hours after xenografting. A cluster of tumor cells forms a lacuna-like space containing erythrocytes. x 2000

in comparison with Nu465 a grade II Ch. An early stage of angiogenesis induction has been correlated with a shorter disease-free period in osteosarcoma (Kaya et al., 2009).

In addition to angiogenic factors, chemokines also play an important role during angiogenic induction. The coexpression of ligands and chemokine receptors in neoplastic cells and extracellular matrix suggests that autocrine and paracrine stimulation by tumor cells results in production of angiogenic factors in response to hypoxia during the first stages of tumor growth, as has been reported in other neoplastic and non-neoplastic conditions (Llombart-Bosch et al., 2003; van der Schaft et al., 2004, 2005; Berghuis et al., 2011). Furthermore, inhibition of some of these molecules has been shown to

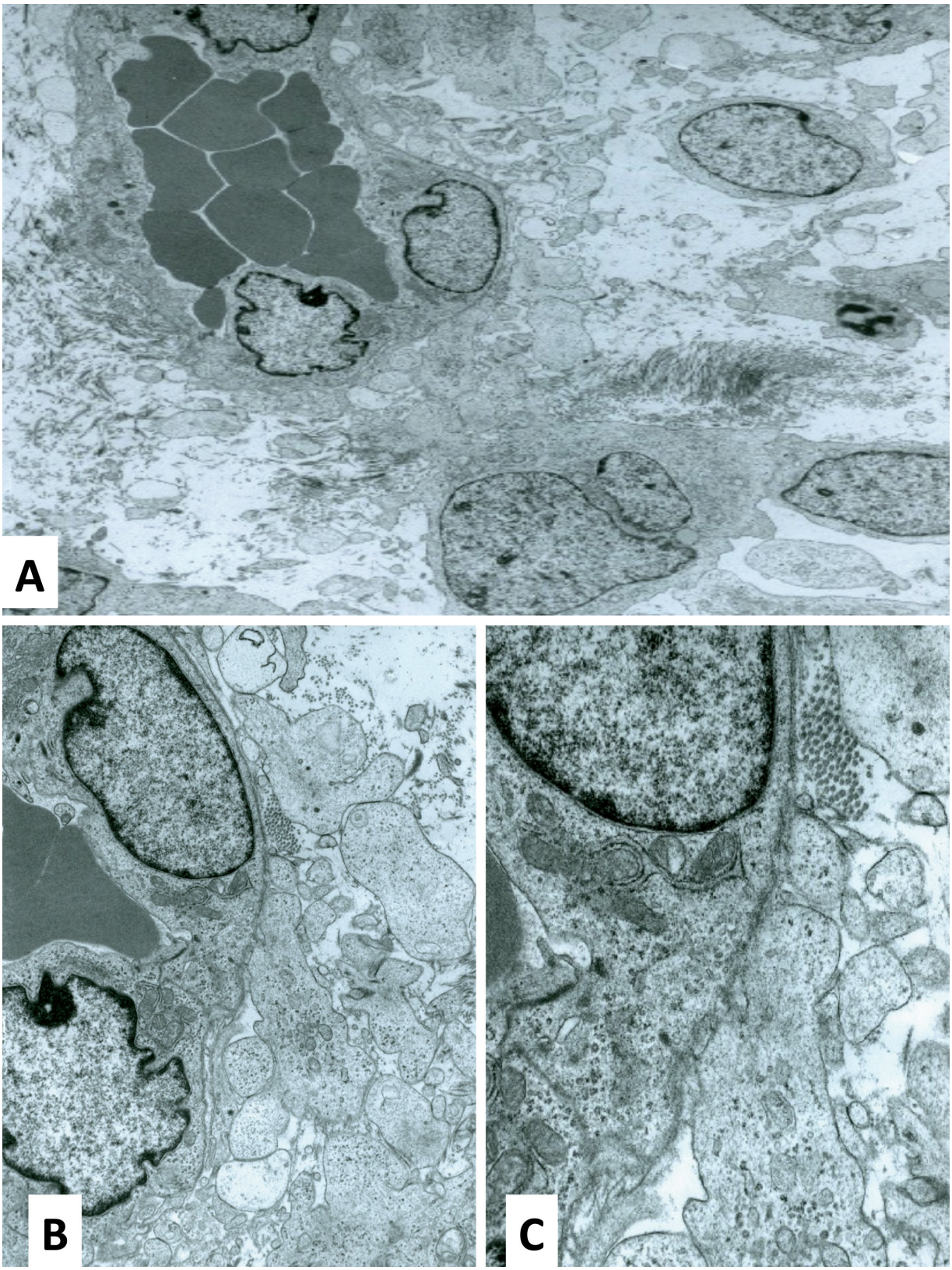

Fig. 6. Electron microscopy of a neoformed vessel within the tumor. **A.** View of the capillary wall composed of host endothelial angioblasts, filled with erythrocytes and surrounded by tumor cells. **B.** Close up view of the endothelial cells and the tumor cell cytoplasm enveloping the vessel. **C.** Higher magnification of the relationship between the neoplastic cells and the endothelia with no interposed basal membranes. A, x 1600; B, x 2000; C, x 5000

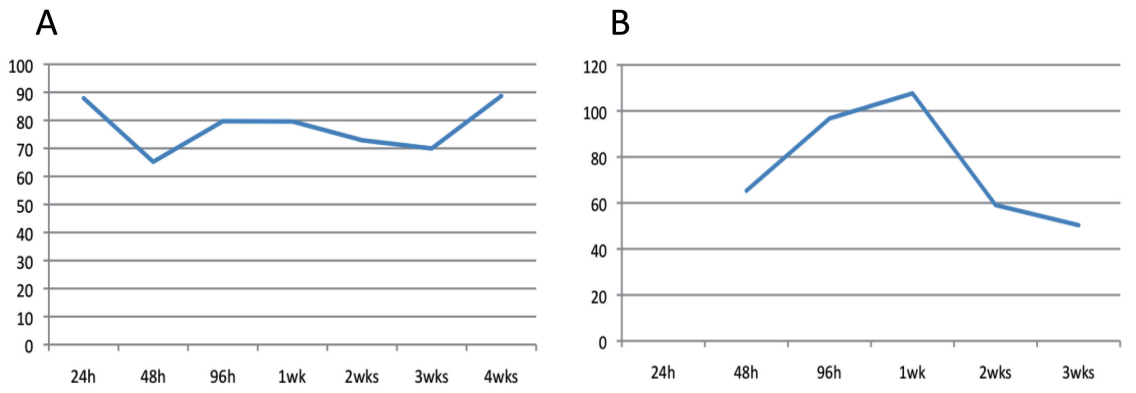

Fig. 7. A. Murine VEGF serum levels by ELISA in the Nu465 series. **B.** Murine VEGF serum levels by ELISA in the Nu467 series. Sample from 4th week in Nu467 was not available for analysis.

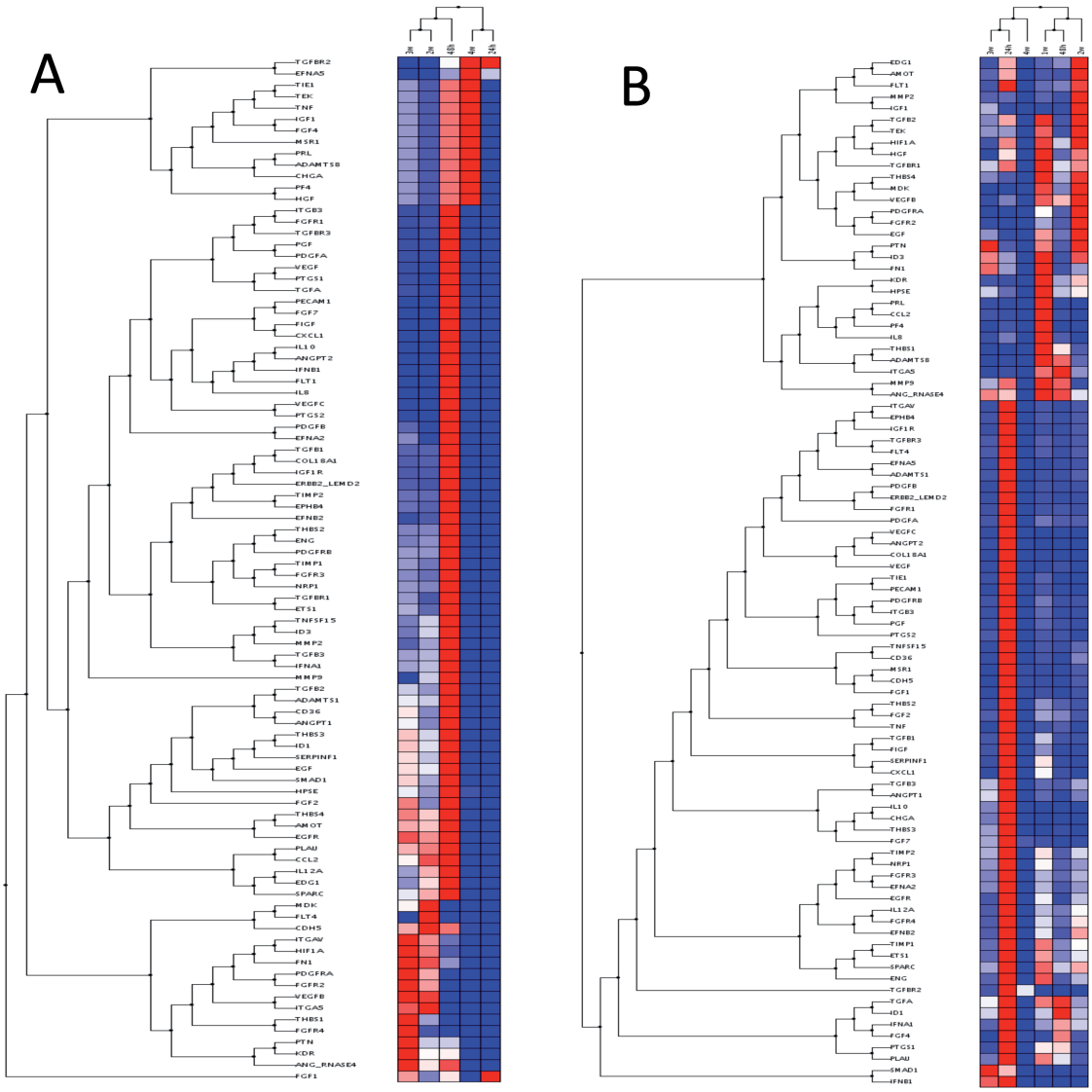

Fig. 8. Cluster tree of genes related to angiogenesis by qRT-PCR obtained from the Nu465 **(A)** and Nu467 **(B)** series using distance correlation and applying a linear correlation coefficient at different times. Overexpressed genes are shown in dark red, underexpressed genes in dark blue and no change in white. Samples from 96h and 1st week in Nu465, and 96h in Nu467 were not available for analysis.

demonstrate an anti-angiogenic effect in Ch (Sun et al., 2013). Some authors have reported that dedifferentiating tumor cells do not acquire sensitivity to angiogenesis inhibitors, suggesting that an anti-angiogenesis protocol may lead to only partial tumor regression (van der Schaft et al., 2004). Consequently, data regarding the relationship between angiogenesis and prognosis in malignant bone tumors remain scarce and controversial (Kubo et al., 2013; Kim et al., 2014). In Ch, high microvessel density seems to be associated with age, high histological grade and poor prognosis, suggesting the development of anti-angiogenic chemotherapy for patients with Ch (Kubo et al., 2013). However, in other tumors, such as osteosarcoma, this factor seems to be associated with a longer overall and relapse-free survival (Kreuter et al., 2004; Kubo et al., 2013). Some authors have suggested exploring possible relationships between presence of vasculogenic structures and response to anti-angiogenesis therapy (van der Schaft et al., 2004; Wu et al., 2014). Furthermore, it is interesting to speculate that anti-angiogenic therapy may result in a selective growth advantage for cells exhibiting vasculogenic mimicry, promoting drug-induced resistance.

Moreover the fact that two grade I Chs did not take or grow in this nude model once more puts into question the true malignancy of this neoplasm.

In conclusion, this model could provide information, not only on the early stages of the angiogenic process in Ch, but also on the efficacy of the new anti-angiogenic targeted therapies. Additionally it offers an excellent way to study tumor angiogenesis in human Ch. The comparative study between two different aggressive Chs revealed a different expression profile of angiogenic factors which may be useful in predicting the behavior and outcome of cartilage-forming tumors. Our results suggest that Grade III Ch (Nu467) might be more responsive to anti-angiogenic therapy. We also demonstrate that angiogenesis is a multi-step process, mainly induced by hypoxia, that involves several molecular factors and cell types at different times. The fact that angiogenesis is a dynamic and changing process over time should be taken into consideration when developing future therapeutic strategies in Ch.

Acknowledgements. The authors thank David Harrison for the English review and editing of the manuscript. This study was supported by grants of the 6th FP of the EC: Prognosis and Therapeutic Targets in the Ewing Family of Tumors (PROTHETS), Contract number: 503036; and EuroBoNeT Network, contract number: 018814, and from the Fundación Instituto Valenciano de Oncología (FIVO), Valencia, Spain.

Conflict of Interest. The authors declare that they have no conflict of interest.

References

Berghuis D., Santos S.J., Baelde H.J., Taminiau A.H., Egeler R.M., Schilham M.W., Hogendoorn P.C. and Lankester A. (2011). Pro-inflammatory chemokine-chemokine receptor interactions within the Ewing sarcoma microenvironment determine CD8(+) T-lymphocyte infiltration and affect tumour progression. J. Pathol. 223, 347-357.

Boeuf S., Bovee J.V., Lehner B., Hogendoorn P.C. and Richter W. (2010). Correlation of hypoxic signalling to histological grade and outcome in cartilage tumours. Histopathology 56, 641-651.

Bovee J.V., Hogendoorn P.C., Wunder J.S. and Alman B.A. (2010). Cartilage tumours and bone development: molecular pathology and possible therapeutic targets. Nat. Rev. Cancer 10, 481-488.

Calabuig-Farinas S., Benso R.G., Szuhai K., Machado I., Lopez-Guerrero J.A., de Jong D., Peydro A., San Miguel T., Navarro L., Pellin A. and Llombart-Bosch A. (2012). Characterization of a new human cell line (CH-3573) derived from a grade II chondrosarcoma with matrix production. Pathol. Oncol. Res. 18, 793-802.

Carmeliet P. and Jain R.K. (2011). Molecular mechanisms and clinical applications of angiogenesis. Nature 473, 298-307.

Chen C., Zhou H., Wei F., Jiang L., Liu X., Liu Z. and Ma Q. (2011). Increased levels of hypoxia-inducible factor-1alpha are associated with Bcl-xL expression, tumor apoptosis, and clinical outcome in chondrosarcoma. J. Orthop. Res. 29, 143-151.

DuBois S. and Demetri G. (2007). Markers of angiogenesis and clinical features in patients with sarcoma. Cancer 109, 813-819.

Gil-Benso R., Lopez-Gines C., Lopez-Guerrero J.A., Carda C., Callaghan R.C., Navarro S., Ferrer J., Pellin A. and Llombart-Bosch A. (2003). Establishment and characterization of a continuous human chondrosarcoma cell line, ch-2879: comparative histologic and genetic studies with its tumor of origin. Lab. Invest. 83, 877-887.

Giner F., Lopez-Guerrero J.A., Machado I., Garcia-Casado Z., Peydro-Olaya A. and Llombart-Bosch A. (2015). The early stages of tumor angiogenesis in human osteosarcoma: a nude mice xenotransplant model. Virchows Arch. 467, 193-201.

Hanahan D. and Weinberg R.A. (2011). Hallmarks of cancer: the next generation. Cell 144, 646-674.

Hogendoorn P.C., Bovée J.V. and Nielsen G.P. (2013). Chondrosarcoma In World Health Organisation Classification of tumours. In: WHO Classification of tumours of soft tissue and bone. Fletcher C.D., Bridge J.A., Hogendoorn P.C. and Mertens F. (eds). Vol. 1. IARC Press, Lyon. pp 264-268.

Kaya M., Wada T., Nagoya S., Sasaki M., Matsumura T. and Yamashita T. (2009). The level of vascular endothelial growth factor as a predictor of a poor prognosis in osteosarcoma. J. Bone Joint Surg. Br. 91, 784-788.

Kim S., Ding W., Zhang L., Tian W. and Chen S. (2014). Clinical response to sunitinib as a multitargeted tyrosine-kinase inhibitor (TKI) in solid cancers: a review of clinical trials. Onco. Targets Ther. 7, 719-728.

Kreuter M., Bieker R., Bielack S.S., Auras T., Buerger H., Gosheger G., Jurgens H., Berdel W.E. and Mesters R.M. (2004). Prognostic relevance of increased angiogenesis in osteosarcoma. Clin. Cancer Res. 10, 8531-8537.

Kubo T., Shimose S., Fujimori J., Arihiro K. and Ochi M. (2013). Diversity of angiogenesis among malignant bone tumors. Mol. Clin. Oncol. 1, 131-136.

Lin C., McGough R., Aswad B., Block J.A. and Terek R. (2004). Hypoxia induces HIF-1alpha and VEGF expression in chondrosarcoma cells and chondrocytes. J. Orthop. Res. 22, 1175-1181.

Link M.P., Goorin A.M., Miser A.W., Green A.A., Pratt C.B., Belasco J.B., Pritchard J., Malpas J.S., Baker A.R., Kirkpatrick J.A., Ayala A.G., Shuster J.J., Abelson H.T., Simone J.V. and Vietti T.J. (1986).

The effect of adjuvant chemotherapy on relapse-free survival in patients with osteosarcoma of the extremity. N. Engl. J. Med. 314, 1600-1606.

Livak K.J. and Schmittgen T.D. (2001). Analysis of relative gene expression data using real-time quantitative PCR and the 2 (-Delta Delta C(T)). Methods 25, 402-408.

Llombart-Bosch A., Lopez-Guerrero J.A., Carda Batalla C., Ruiz Suari A. and Peydro-Olaya A. (2003). Structural basis of tumoral angiogenesis. Adv. Exp. Med. Biol. 532, 69-89.

Machado I., Giner F., Mayordomo E., Carda C., Navarro S. and Llombart-Bosch, A. (2008). Tissue microarrays analysis in chondrosarcomas: light microscopy, immunohistochemistry and xenograft study. Diagn. Pathol 3 (Suppl 1), S25.

Mantadakis E., Kim G., Reisch J., McHard K., Maale G., Leavey P.J. and Timmons C. (2001). Lack of prognostic significance of intratumoral angiogenesis in nonmetastatic osteosarcoma. J. Pediatr. Hematol. Oncol. 23, 286-289.

Ohba T., Cates J.M., Cole H.A., Slosky D.A., Haro H., Ando T., Schwartz H.S. and Schoenecker J.G. (2014). Autocrine VEGF/VEGFR1 signaling in a subpopulation of cells associates with aggressive osteosarcoma. Mol. Cancer Res. 12, 1100-1111.

Pinto S., Martinez-Romero A., O'Connor J.E., Gil-Benso R., San-Miguel T., Terradez L., Monteagudo C. and Callaghan R.C. (2014). Intracellular coexpression of CXC- and CC-chemokine receptors and their ligands in human melanoma cell lines and dynamic variations after xenotransplantation. BMC Cancer 14, 118.

Rozeman L.B., Cleton-Jansen A.M. and Hogendoorn P.C. (2006). Pathology of primary malignant bone and cartilage tumours. Int. Orthop. 30, 437-444.

Sun X., Charbonneau C., Wei L., Yang W., Chen Q. and Terek R.M. (2013). CXCR4-targeted therapy inhibits VEGF expression and chondrosarcoma angiogenesis and metastasis. Mol. Cancer Ther. 12, 1163-1170.

van der Schaft D.W., Hillen F., Pauwels P., Kirschmann D.A., Castermans K., Egbrink M.G., Tran M.G., Sciot R., Hauben E., Hogendoorn P.C., Delattre O., Maxwell P.H., Hendrix M.J. and Griffioen A.W. (2005). Tumor cell plasticity in Ewing sarcoma, an alternative circulatory system stimulated by hypoxia. Cancer Res. 65, 11520-11528.

van der Schaft D.W., Seftor R.E., Seftor E.A., Hess A.R., Gruman L.M., Kirschmann D.A., Yokoyama Y., Griffioen A.W. and Hendrix M.J. (2004). Effects of angiogenesis inhibitors on vascular network formation by human endothelial and melanoma cells. J. Natl. Cancer Inst. 96, 1473-1477.

van Oosterwijk J.G., Anninga J.K., Gelderblom H., Cleton-Jansen A.M. and Bovee J.V. (2013). Update on targets and novel treatment options for high-grade osteosarcoma and chondrosarcoma. Hematol. Oncol. Clin. North. Am. 27, 1021-1048.

Wu M.H., Huang C.Y., Lin J.A., Wang S.W., Peng C.Y., Cheng H.C. and Tang C.H. (2014). Endothelin-1 promotes vascular endothelial growth factor-dependent angiogenesis in human chondrosarcoma cells. Oncogene 33, 1725-1735.

Accepted February 3, 2017